likely have different origins. The fact that the T Tau system is almost unique in showing extended H_2 emission could (a) be related to the presence of a jet interacting with the local environment (Burnham's Nebula and its northern counterpart), and (b) be related to a relatively massive circumbinary disk and a binary system with a component orbital speed of the same order as is necessary to shock excite molecular hydrogen (5 km/s) in this disk.

5. Future Prospects

The high angular resolution afforded by SHARP II and ADONIS has enabled us to study the distribution of warm molecular hydrogen in the T Tauri system in considerably more detail than has been possible before. With multi-line observations it is possible to determine the excitation mechanism. The ratio of the (v = 1 – 0) S(1), (v = 2 – 1) S(1), and e.g. (v = 9 – 7) 0(3) near-IR lines can be taken to distinguish between UV fluorescence and shock excitation, and to determine the gas temperature in the latter case. From their integral field spectroscopy with 3D, Herbst et al. (1996) conclude that the bulk of the material is shock excited with a typical temperature of $\sim$ 2000 K. Future observations of the (v = 2 – 1) S(1) and (v = 9 – 7) O(3) with SHARP II and ADONIS could be used to map the gas temperature at higher spatial resolution, and to search for fluorescent H_2, whose presence is expected on the basis of IUE observations of UV fluorescence (Brown et al., 1981). Even more efficiently, such observations could be performed with the 3D integral field spectrometer, which will be coupled to the ALFA adaptive optics system on Calar Alto in the course of 1997. In addition to the multiplex advantage of 3D, the strictly simultaneous spectra will allow a much better continuum subtraction, and thus a better definition of the emission close to the two bright stars.

Acknowledgements

We thank the ESO staff on La Silla for their excellent support during our observing run. We are particularly indebted to Frank Eisenhauer, who built the SHARP II camera and calibrated its scanning Fabry-Perot etalon, for his expert advice on observing strategy and data reduction.

References

Artymowicz, P., & Lubow, S.H. (1996), *ApJ* **467**, L77.
Beckwith, S., Gatley, I., Matthews, K., & Neugebauer, G. (1978), *ApJ* **223**, L41.
Brown, A., Jordan, C., Millar, T.J., Gondhalekar, P., & Wilson, R. (1981), *Nature* **290**, 34.
Bührke, T., Brugel, E.W., & Mundt, R. (1986), *A&A* **163**, 83.
Carr, J.S. (1990), *AJ* **100**, 1244.
Dyck, H.M., Simon, T., & Zuckerman, B. (1982), *ApJ* **255**, L103.
Ghez, A.M., Neugebauer, G., Gorham, P.W., Haniff, C.A., Kulkarni, S.R., Matthews, K., Koresko, C., & Beckwith, S. (1991), *AJ* **102**, 2066.
Herbst, T.M., Beckwith, S.V.W., Glindemann, A., Tacconi-Garman, L.E., Kroker, H., & Krabbe, A. (1996), *AJ* **111**, 2403.
Koresko, C.D., Herbst, T.M., & Leinert, Ch. (1997), *ApJ*, in press.
Momose, M., Ohashi, N., Kawabe, R., Hayashi, M., & Nakano, T. (1996), *ApJ* **470**, 1001.
Nakajima, T., & Golimowski, D.A. (1995), *AJ* **109**, 1181.
Robberto, M., Clampin, M., Ligori, S., Paresce, F., Sacca, V., & Staude, H.J. (1995), *A&A* **296**, 431.
Schwartz, R.D. (1975), *ApJ* **195**, 631.
Smith, M. D., & Brand, P. W. J. L. (1990), *MNRAS* **242**, 495.
Solf, J., Böhm, K.-H., & Raga, A. (1988), *ApJ* **334**, 229.
van Langevelde, H.J., van Dieshoeck, E.F., van der Werf, P.P., & Blake, G.A. (1994), *A&A* **287**, L25.
Weintraub, D.A., Kastner, J.H., Zuckerman, B., & Gatley, I. (1992), *ApJ* **391**, 784.
Weintraub, D.A., Masson, C.R., & Zuckerman, B. (1989), *ApJ* **344**, 915.
Zinnecker, H., & Wilking, B.A. (1992), in *Binaries as tracers of Stellar Formation,* Eds. Duquennoy, A., & Mayor, M., Cambridge Univ. Press, p. 269.

Examples of High-Resolution Imaging and Polarimetry of R Monocerotis and NGC 2261

N. AGEORGES, J. R. WALSH, ESO

1. Introduction

High angular resolution polarisation and surface brightness images of R Monocerotis (R Mon) and its associated reflection nebulae NGC 2261 (Hubble's variable nebula), have been obtained. Ground-based optical imaging and near-infrared polarimetric data as well as HST optical polarisation measurements are presented as examples of current high-resolution imaging capabilities.

R Mon is a variable semi-stellar object, which has never been resolved into a single star. It is presumed to be a very young star in the process of emerging from its parent cloud and the source of illumination of the nebula. For decades the variability of both R Mon, and NGC 2261, has been observed both in brightness and polarisation (Hubble, 1916; Lightfoot, 1989). The apparent cometary nebula NGC 2261 extends, in the optical $\approx 3'$ northward of R Mon. CO mapping (Canto et al., 1981) reveals that it is indeed one lobe of a bipolar nebula; the southern lobe being obscured by the presumed tilted disk around R Mon. Some 7′ north of R Mon there are a group of associated Herbig-Haro objects (HH39). A faint loop extending between HH39 and the eastern extremity of NGC 2261 has been interpreted by Walsh & Malin (1985) as evidence of a stellar wind driven flow between R Mon and HH39. Imhoff & Mendoza (1974) derived a luminosity of 660 $L_\odot$ for R Mon, assuming a distance of 800 pc (Walker, 1964), which is atypical of the low luminosity normally observed for Herbig-Haro exciting sources. There is also a faint jet-like feature south of R Mon (Walsh & Malin, 1985); this is not a true jet but dust illuminated by radiation escaping from the dusty disk around R Mon (Warren-Smith et al., 1987).

In this article we present new observational data at high spatial resolution and discuss some possible explanations of the features revealed. These data serve to illustrate the state of the art in high angular resolution polarimetry. The observations have been acquired both from the ground with SUSI and ADONIS at ESO-Chile and from space with the Hubble Space Telescope. In section 2 we present in some detail the observational procedures. Some results are shown in section 3 and we end by a short discussion on R Mon and NGC 2261 together with some comments on the potential of high-resolution polarimetry.

2. Observations

NGC 2261 has been adopted as an HST polarisation calibrator (Turnshek et al., 1990), since it is extended, has high polarisation ($\gtrsim$ 10%) and has been well observed from the ground (see e.g. Aspin et al., 1985 and Minchin et al., 1991). The ADONIS and HST polarimetric data of R Mon and NGC 2261 presented here were acquired in order to calibrate polarimetric data of other

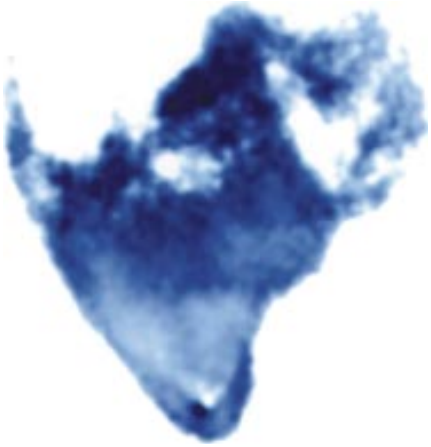

Figure 1: Hα – V SUSI colour map. In this figure, white corresponds to blue physical colour and black to redder colour. North is to the top and east to the left. The size of the image is ∼ 2′ × 2′. North is to the top and east to the left.

astronomical sources; however, we show that the high resolution of the data reveals new details of this fascinating source.

2.1 Ground-based optical observations

Ground-based optical observations were made with the SUperb Seeing Imager (SUSI) of ESO, at the NTT in April 1996. The Tek CCD chip of SUSI has 1024 × 1024 pixels, each with a size of 0.13″, giving a 2′ field of view. These observations are typical of 'passive' imaging. An advantage is that a large field can be observed, but the disadvantage is that the spatial resolution is at the mercy of the seeing variations. Indeed the V and Hα band data presented here have been acquired under the worst seeing conditions (average 1.2″) compared to the other data and thus have the lowest resolution.

Images in V and a narrow-band (60 Å wide) Hα filter with exposure times of 60 seconds were obtained. The data have been flat fielded and then flux calibrated in MIDAS. In the absence of a real flux calibrator observed during these observations, and in order to be able to create the colour (Hα–V) map, the integrated flux in a 5″ aperture centred on R Mon was compared with the equivalent magnitudes from Aspin, McLean & Coyne (1991). This calibration does not allow accurate photometric information to be derived, since R Mon is known to be variable (e.g. 4 magnitudes in 1 year – Matsumara & Seki, 1995) on short and long time scales. The calibration is however sufficient for the purposes of scaling the colour map.

2.2 Near-infrared observations

The near-infrared polarimetric data were acquired in March 1996 with the ESO adaptive optics instrument, ADONIS, on the 3.6-m telescope. The camera is a 256 × 256 pixels NICMOS3 array and a pixel scale of 0.05″/pixel was used for the observations, giving a field of 25″ × 25″ (see the ADONIS home page http://www.ls.eso.org/lasilla/Telescopes/360cat/html/ADONIS/ for details). In the case of these observations, the resulting images are only partially affected by the seeing effects. The data presented are the first example of scientific use of polarisation measurements coupled with the ADONIS adaptive optics system.

As point spread function (PSF) and polarisation calibrator, the nearby unpolarised star HD 64299 was employed. Table 1 indicates the number of frames observed, per position of the polariser, for a given wavelength and integration time for both the reference star and R Mon. Nine positions of the polariser were used for each series of observations: from 0° to 157.5° in steps of 22.5° and 0° again to finish the sequence. The first and last images were compared in order to check the photometric stability. The basic data reduction (dead pixel correction, flat fielding, sky subtraction, stacking of images) were performed with ECLIPSE – an image-processing engine developed at ESO for astronomical data reduction in general and ADONIS data in particular. For further information on ECLIPSE see: http://www.eso.org/~ndevilla/adonis/eclipse. At each pixel, or set of binned pixels, a cosine function was fitted to the values as a function of polariser position angle, and maps of the mean signal, linear polarisation and polarisation position angle were computed for both the R Mon and HD 64299 data using a dedicated MIDAS programme. A value of the instrumental polarisation of 2.7% ± 0.2% at 158 ± 2° was derived at J, with the errors based on the image statistics. We consider this as a preliminary value until all the calibration data on unpolarised and polarised standard stars have been analysed. The polarisation and position angle of the polarisation vectors shown in the maps will change slightly upon adoption of an improved instrumental polarisation.

2.3 Optical HST observations

The WFPC2 imager aboard HST consists of four 800^2 CCD chips – three Wide Field (0.1″ pixels) and one Planetary Camera (0.046″ pixels). There is a polariser filter which is a quad of four polarisers oriented at different angles (see the WFPC2 Instrument Handbook for details). Data can be taken by either rotating the filter over a single chip or by taking images in successive chips. The advantage of space observations is that the PSF is constant in time, but, in the case of WFPC2, it is spatially varying (on account of the correction for the spherical aberration of the telescope). The resolution is therefore high but not diffraction limited since the PC pixels undersample the PSF.

As part of the calibration programme for this instrument, images of R Mon and NGC 2261 were taken in February 1995 in both modes, together with an unpolarised standard (G191B2B) and a polarised standard (BD+64°106). The PI was W. Sparks (Programme ID 5574). Images taken with the POLQ filter (in which each chip is imaged by the polariser at a different rotation 0,45, 90 and 135°) were studied. A set of F555W (V band) and F675W (R band) filter images were analysed, all with 300s exposure. The field of the three WFC chips is 80 × 80″ but the field of the PC chip is 35 × 35″ and, since the data from all four chips were used, the image area was restricted. The polarisation in R Mon and the brightest portions of NGC 2261 was mapped. However, the HST polarisation maps do not give adequate data over R Mon itself since R Mon occurs close to the edge of the PC chip in a region where there is cross-talk between the polariser quad filters.

3. Results

3.1 SUSI data

Figure 1 shows an Hα–V colour map of NGC 2261 from the SUSI images. The map has been convolved by a 3 pixel wide Gaussian to smooth the observed structures. The colour map shows a region of redder colour (coded in black in Fig. 1) just to the south of R Mon and two spikes of bluer colour extending NE and NW, with the bluer one to the NE. There are some small spatial colour changes in the NGC 2261 nebula in addition.

3.2 ADONIS data

On account of their short integration times, the total flux ADONIS images, at J, H and K, do not show much detail of NGC 2261. Some extension north-east of the bright source appears with de-

	R Mon		HD 64299	
	# Frames	τ (s)	# Frames	τ (s)
J	10	1	10	5
H	20	0.4	10	3
K	10	0.1	10	3

TABLE 1: Observational details of the ADONIS data taken for R Mon and the unpolarised reference star HD 64299. Columns 2 and 4 indicate the total number of frames acquired per position of the polariser; columns 3 and 5 the respective integration time per frame.

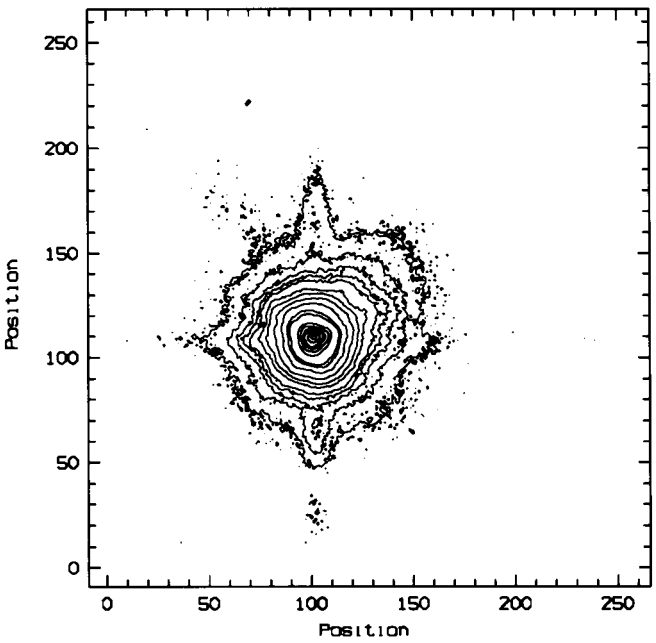

Figure 2: Intensity contour plot of the observed ADONIS K band averaged image of R Mon. North is to the top and left to the east. The scale is in pixels (0.05″/pixel). The trace of the telescope spider is well seen at the lowest plotted contour level. The central contours point out the residual coma in our data as well as a slight East-West elongation.

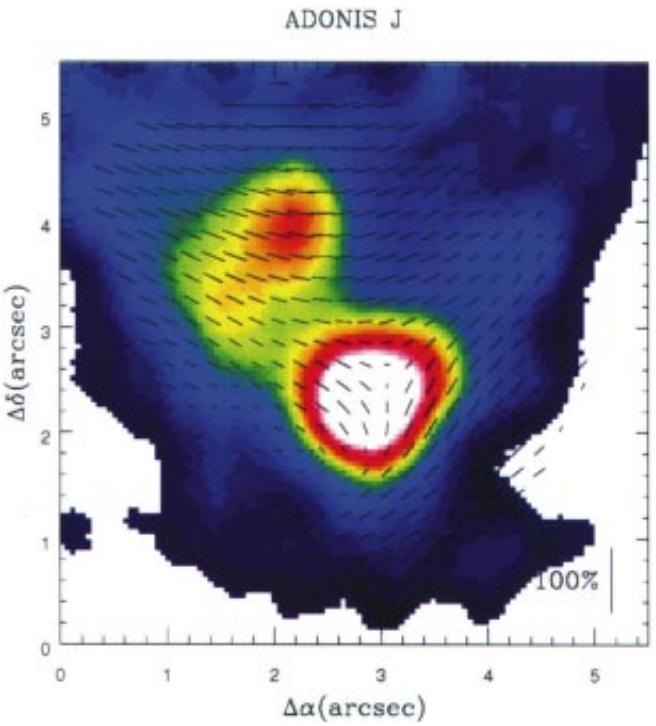

Figure 3: ADONIS J band restored image with the polarisation vector plot superposed. For this plot the polarisation vectors have been calculated in square apertures of 0.4″ radius.

creasing wavelength. In the K band image (see Fig. 2) the spider of the telescope is clearly recognisable at a level of up to 0.09% of the peak intensity. Two other optical effects can be noticed in this image: an elongation along the X-axis, which results from a vibration in this direction, whose origin is not clear; the triangular shape of the PSF, which is a residual triangular coma. This last effect, linked to a servo-loop problem, appears at poor correction level and is not repeatable.

In order to increase the effective resolution of the images, deconvolution with the star HD 64299 used as PSF calibrator, by the Lucy-Richardson algorithm (Lucy, 1974) was applied. After only 10 iterations, the nebular structure around R Mon is apparent at a level of 0.14% of the peak intensity in J Band for example. Figures 3, 4, 5 show colour plots of the restored J, H and K images. Two distinct 'knots' north-east of R Mon are revealed in all IR images and another to the NW in the J band image. These knots are also seen in the HST V and R images; the NW knot is the same as the NW spike mentioned in section 3.1.

3.3 HST data

The WFPC2 data for R-Mon had to be recalibrated since the original data were

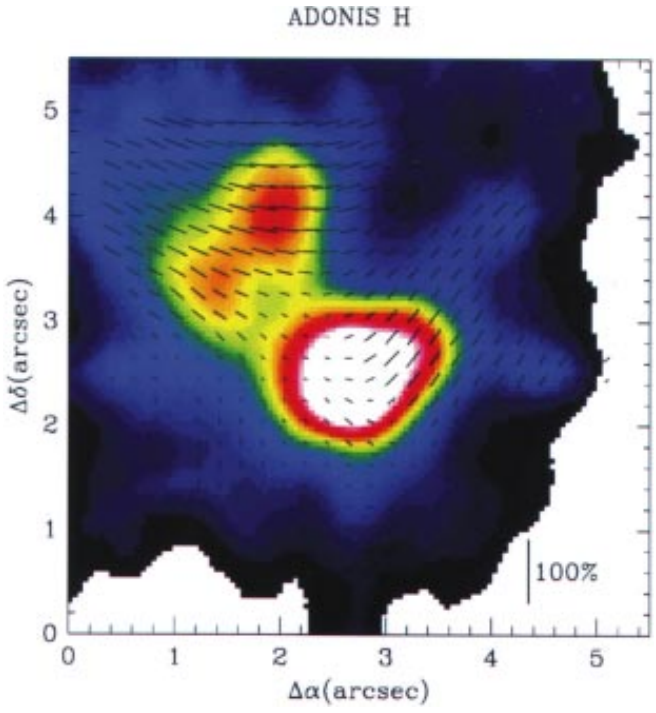

Figure 4: Same as Figure 3 but in H band.

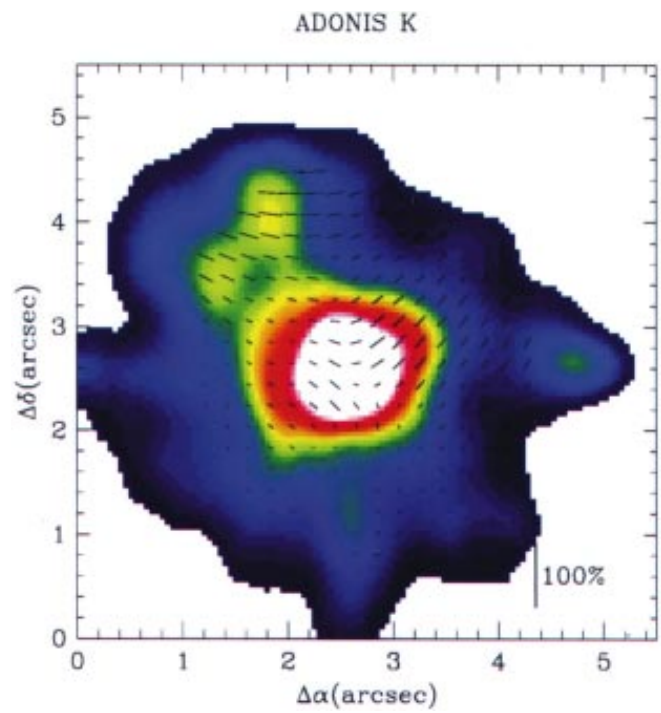

Figure 5: Same as Figure 3 but in K band.

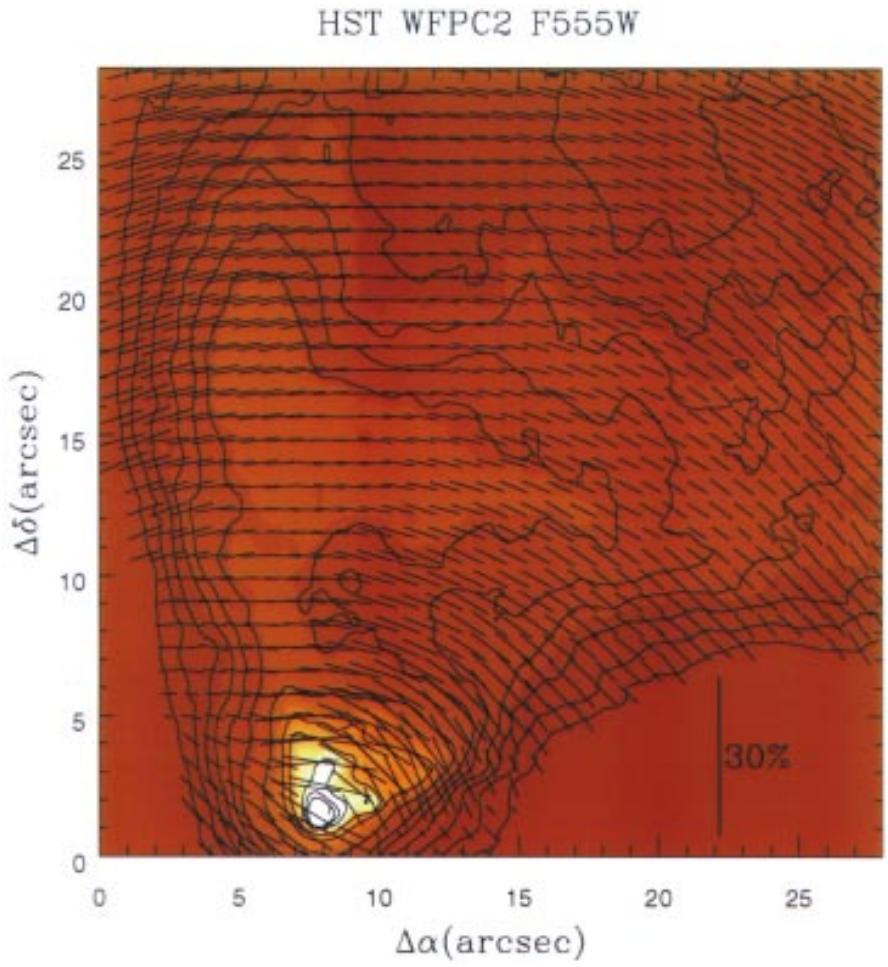

Figure 6: HST V band polarisation map, convolved to a 0.8″ resolution, overplotted on an intensity map of 0.1″ resolution. The orientation in this image is tilted at position angle 15° compared to the previous images, where north is to the top and east to the left.

respectively, show the V and large R band total flux image and the deduced polarisation map as a vector plot.

4. Discussion

R Mon is known to have Hα emission (e.g. Stockton et al., 1975) which is then scattered by dust in the reflection nebula; there is no convincing evidence for intrinsic line emission in the nebula and the polarisation is very similar at Hα and V (Aspin et al., 1985). The SUSI Hα – V colour map (Fig. 1) then traces small differences in extinction through the nebula, differences in scattered flux arising from different scattering angles and possibly also multiple scattering in the near vicinity of R Mon itself. Interpretation of these colour changes is complex since R Mon itself also shows temporal colour changes and these then propagate through reflection over the nebula. The 'structural' changes observed in

taken before flat fields with the polariser filters were available. The WFPC2 Web pages give full details of flat fielding WFPC2 polariser images and understanding the data (http: //www.stsci.edu/ftp/instrument_news/WFPC2/Wfpc2_pol/wfpc2_pol_cal.html).

The images were corrected for the geometrical distortion and difference in pixel size for the different chips using the standard WFPC2 software in IRAF/STSDAS (wmosaic). The data were handled in the conventional manner: Stokes Q and U parameters were calculated from the difference of the 0 and 90° frames and the 45 and 135° frames respectively. The total flux (sum of polarised and unpolarised), linear polarisation and polarisation position angle were calculated from the Stokes parameters. The errors on the Stokes parameters were calculated based on the image statistics and propagated to the polarisation and position angle. The data for the polarized and unpolarised standards were treated in the same way. The deduced instrumental polarisation is about 2.5% for F555W. Dedicated software (written in MIDAS) produces the polarisation maps allowing the data to be binned to increase the signal-to-noise per pixel and cosmic rays to be rejected. Figures 5 and 6,

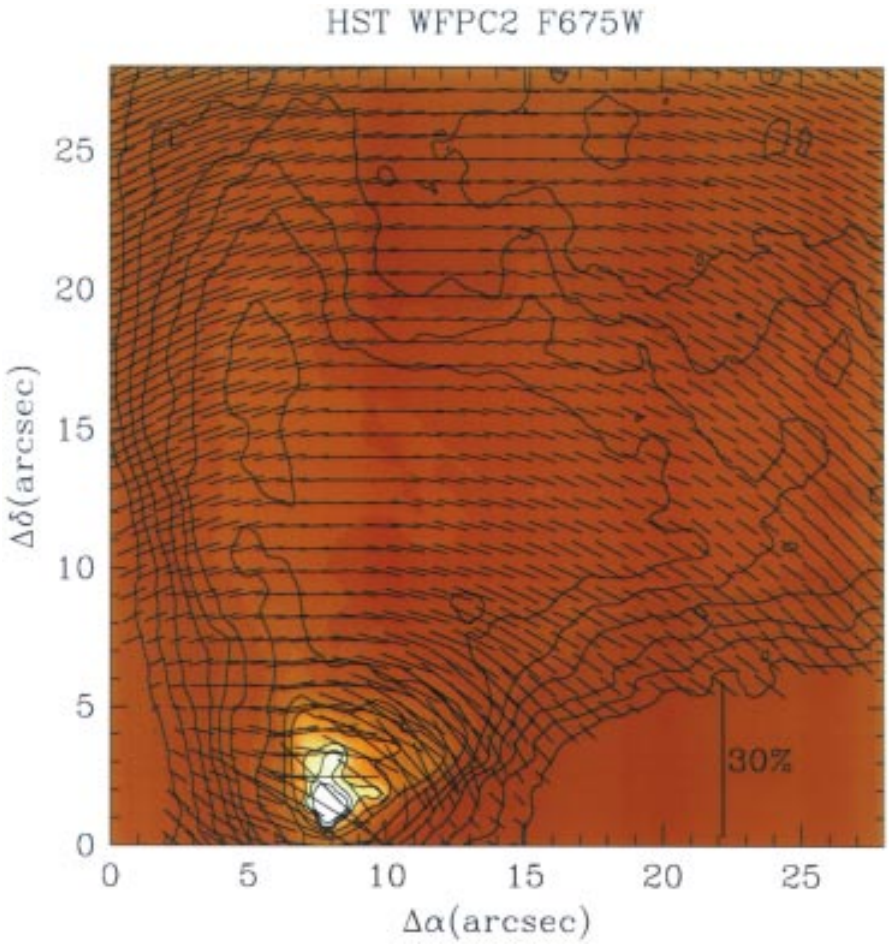

Figure 7: Same as Figure 6 but in large R band.

NGC 2261 are considered to be due to the movement of obscuring clouds in the near vicinity of the embedded stellar source which modulate the illumination escaping in the direction of NGC 2261 ("shadowplay" – Lightfoot, 1989).

The most prominent features on the HST images are the lack of a resolved stellar source to R Mon and the two spikes emanating from it. The eastern spike is present at all wavelengths in the images presented here from V to K band. It is clearly a dust feature or a tunnel of lower obscuration from R Mon into the nebula. The polarisation behaviour of these two spikes could prove useful in studying their origin. The NE spike, extended both in length and width, shows higher linear polarisation (25% at V integrated over its area) with a trend to increased polarisation outwards from R Mon. The NW spike, has lower polarisation (12% at V, and fairly constant along its length), is narrow (0.3″) and not visible in the H and K ADONIS images; Figs. 4, 5). The polarisation position angles of both features are quite consistent with illumination by R Mon. An interpretation of the lower polarisation (of the NW knot) could be in terms of the (single) scattering angle of the radiation from R Mon, reflected off the dust features towards the observer. The NE spike then is more tilted away from the observer than the NW spike. The features could be either 'tubes' relatively free of dust within the extended dust disk about R Mon or individual clumps. An extended cloud would reflect light at different angles giving rise to differing polarisation along its length whilst a radial feature should produce similar polarisation along its whole length (assuming single Mie scattering). However, Scarrott et al. (1989) have studied the polarisation behaviour of the disk around R Mon and suggest that scattering of polarised light and perhaps magnetically aligned grains may play a role. Detailed modelling is required to resolve these differing interpretations but the long wavelength coverage and comparable high resolution (0.2″) polarimetry offered by HST and ADONIS bring critical data to this problem.

Polarisation mapping has been applied to a great variety of astronomical sources: reflection nebulae around young stars, AGB stars, proto-planetary and planetary nebulae; to galactic scale extended emission-line regions in radio galaxies and normal and dusty galaxies; synchrotron sources in supernova remnants and quasars and AGN. Most studies have been at modest spatial resolution dictated by ground-based seeing. However, the application of adaptive optics to polarimetry brings a powerful tool to study the nearby regions of dusty sources enabling the study of dust structures around AGN, non-axially symmetric outflows near AGB stars and dust disks around young stars for example. NICMOS will also enable high-resolution polarimetry to be achieved in J and H bands. HST with WFPC2 allows high-resolution optical imaging in the optical and with the Advanced Camera for Surveys (ACS, see http://jhufos.phajhu.edu/ for details) installed into HST in 1999, even higher resolution polarimetry over a longer wavelength range (2500 to 8200 Å) will be achievable. Polarimetry brings critical data related to orientation that cannot be gained in other ways, and is therefore an important tool for deeper understanding of structures surrounded by dust.

5. Acknowledgements

We would like to thank the ADONIS team for their excellent assistance at the telescope and for the smooth working of the instrument. We also thank John Biretta, at STScI, for helpful discussions on WFPC2 polarimetry.

References

Aspin C., McLean I.S., Coyne G.V., 1985, *AA* **149**, 158.
Canto J., Rodriguez L.F., Barral J.F., Carral P., 1981, *ApJ* **244**, 102.
Hubble, E. P., 1916, *ApJ* **44**, 19.
Imhoff C.L., Mendoza, V.E.E., 1974, *Rev. Mexicana Astr. Ap.* **1**, 25.
Lightfoot, J.F., 1989, *MNRAS* **239**, 665.
Lucy, L.B., 1974, *AJ*, **79**, 745.
Matsumara M., Seki M., 1995, *Astroph. and Space Sci.* **224**, 513.
Minchin N.R. et al., 1991, *MNRAS* **249**, 707.
Scarrott, S.D.M., Draper, P.W., Warren-Smith, R. F., 1989, *MNRAS* **237**, 621.
Stockton, A., Chesley, D., Chesley, S., 1975, *ApJ* **199**, 406.
Turnshek, D.A., Bohlin, R.C., Williamson, R.L., Lupie, O.L., Koornneef, J., Morgan, D.H., *AJ*, **99**, 1243.
Walsh J.R., Malin D.F., 1985, *MNRAS* **217**, 31.
Warren-Smith, R.F., Draper, P.W., Scarrott, S.M., 1987, *ApJ*, **315**, 500.

Proper Motion as a Tool to Identify the Optical Counterparts of Pulsars: the Case of PSR0656+14

R. MIGNANI[1, 3], P.A. CARAVEO[3] AND G.F. BIGNAMI[2, 3]

[1] Max-Plack-Institut fur Extraterrestrische Physik, Garching
[2] Dipartimento di Ingegneria Industriale, Università di Cassino
[3] Istituto di Fisica Cosmica del CNR, Milan

1. Introduction

Up to now, about 1% of Isolated Neutron Stars (INS) have been observed in the optical domain (Caraveo, 1996). From an observational point of view, INSs are challenging targets owing to their intrinsic faintness. Young ($\tau \lesssim 10^4$ yrs) pulsars like the Crab, PSR 0540-69 and Vela are relatively bright, powered by magnetospheric processes, and easily identified through the detection of optical pulsations. However, such magnetospheric emission fades away rapidly in the optical domain, giving way to the star's surface thermal emission. It is the case of the so-called "Middle-Aged" ($\tau \sim 10^5$ yrs) Isolated Neutron Stars (MINSs) that, with a temperature T $\approx 10^5$–10^6 K, can be detected at optical wavelengths as thermal emitters. However, since neutron stars are extremely compact objects (10 km in radius), the optical luminosity of MINSs turns out to be very faint, preventing the timing of their optical emission.

Thus, for MINSs the optical identification generally relies on the positional coincidence with a candidate as well as on its peculiar colours. This is how the candidate counterparts of Geminga (Bignami et al, 1987), PSR 1509-58 (Caraveo et al., 1994b), PSR 0656 +14 (Caraveo et al., 1994a) and PSR 1055-52 (Mignani et al., 1997a; Mignani et al., 1997b) were singled out. However, for some of the closer objects (d ≤ 500 pc) other, independent, pieces of evidence can be collected.

Isolated Neutron Stars are known to be high-velocity objects (Lyne and Lorimer, 1994; Caraveo, 1993), moving in the sky with transverse velocities $v_T \sim$ 100–400 km/s. A tentative optical identification can thus be confirmed, or, at least made much more compelling, by measuring the proper motion, if any, of the optical counterpart. Indeed, this is how the optical identification of Geminga was confirmed by Bignami et al. (1993). In the case of a radio pulsar, with known